Nanoscale

COMMUNICATION

View Article Online
View Journal | View Issue

Cite this: *Nanoscale*, 2019, **11**, 22743

Received 9th August 2019,
Accepted 25th October 2019

DOI: 10.1039/c9nr06859g

rsc.li/nanoscale

Orbital design of topological insulators from two-dimensional semiconductors†

Lei Gao, ‡[a] Jia-Tao Sun,‡[a,b] Gurjyot Sethi,[c] Yu-Yang Zhang, [a,d] Shixuan Du*[a,d] and Feng Liu*[c]

Two-dimensional (2D) materials have attracted much attention because they exhibit various intrinsic properties, which are, however, usually not interchangeable. Here we propose a generic approach to convert 2D semiconductors to 2D topological insulators (TIs) *via* atomic adsorption. The approach is underlined by an orbital design principle that involves introducing an extrinsic s-orbital state of the adsorbate into the intrinsic sp-bands of a 2D semiconductor, so as to induce s–p band inversion for a TI phase, as demonstrated by tight-binding model analyses. Based on first-principles calculations, we successfully apply this approach to convert CuS, CuSe and CuTe into TIs by adsorbing one adatom per unit cell of Na, $Na_{0.5}K_{0.5}$ and K as well as Rb and Cs. Moreover, if the chalcogens in the 2D semiconductor have a decreasing ability of accepting electrons, the adsorbates should have an increasing ability of donating electrons. Our findings open a new door to discovering TIs by predictive material design beyond finding preexisting TIs.

Recently, two-dimensional (2D) materials have attracted much attention for both fundamental interest and their potential applications.[1–4] So far, a suite of different classes of 2D materials have been discovered, ranging, *e.g.*, from inorganic Dirac semimetals,[5,6] semiconductors,[7,8] topological insulators (TIs),[9–12] superconductors[13] and ferromagnets,[14] to their organic counterparts.[15–18] Although some efforts have been made to tune the intrinsic properties of 2D materials, such as by strain[19] and alloying,[20] usually different classes of 2D materials are not interchangeable. Here we propose a generic approach to convert 2D semiconductors, which are amply abundant, to 2D TIs, which are relatively less available, *via* surface adsorption and strain engineering.

Because of a very large surface area, 2D materials are extremely sensitive to surface modification,[21,22] while their unltrathinness makes them very sensitive to strain.[22–24] This offers them a unique advantage over their 3D counterparts, as the intrinsic properties of the whole 2D materials can in principle be modified through adsorption and/or strain engineering so that one class of 2D materials may be converted into another class. Below we demonstrate this possibility by converting 2D semiconductors into TIs predominantly by surface adsorption where one alkali atom is introduced into each unit cell of the 2D semiconductor to completely change its intrinsic band structure and band topology, which is apparently impossible for 3D materials.

We will first illustrate our approach, which is underlined by an orbital design principle, using a tight-binding (TB) model[25] that represents a typical 2D sp-band semiconductor in a trigonal lattice. Their top of the valence band and bottom of the conduction band mainly consist of p- and s-states, respectively. An extrinsic s-state of alkali metals with appropriate energy is brought in to induce s–p band inversion to form a TI phase; a generic phase diagram is constructed in the parameter space of energy levels and spin–orbit coupling (SOC). Then, using first-principles calculations, we demonstrate this approach for real materials by converting the semiconducting monolayer CuS and CuTe into a TI *via* adsorbing Na and K respectively with an appropriate s-level energy, and CuSe into a TI *via* adsorbing a mixture of Na and K with a tuned s-level energy or by adsorbing either Na or K on a strained CuSe *via* a tuned p-level valence-band edge. Also, adsorption of Rb and Cs can work similarly.

We prescribe this concept of orbital design principle in a three-site (alkali metal adsorbate, cation and anion in a compound semiconductor) and four-band (s_1 from the adsorbate, s_2, p_x and p_y from the 2D semiconductor) TB model.

[a]*Institute of Physics & University of Chinese Academy of Sciences, Chinese Academy of Sciences, Beijing 100190, P.R. China. E-mail: sxdu@iphy.ac.cn*
[b]*School of Information and Electronics, Beijing Institute of Technology, Beijing 100081, China*
[c]*Department of Materials Science and Engineering, University of Utah, Salt Lake City, Utah 84112, USA. E-mail: fliu@eng.utah.edu*
[d]*CAS Center for Excellence in Topological Quantum Computation, Beijing 100190, P.R. China*

†Electronic supplementary information (ESI) available. See DOI: 10.1039/c9nr06859g

‡Contributed equally.

Expanding to the first-order of k around the Γ point, the spinless Hamiltonian reduces to

$$H = \begin{pmatrix} \varepsilon_{s_1} + 6t_{s_1s_1\sigma} & 3t_{s_1s_2\sigma} & -\frac{\sqrt{3}}{4}t_{s_1p\sigma}(ik_x + k_y) & -\frac{\sqrt{3}}{4}t_{s_1p\sigma}(ik_x - k_y) \\ & \varepsilon_{s_2} + 6t_{s_2s_2\sigma} & -\frac{\sqrt{3}}{2}t_{s_2p\sigma}(ik_x + k_y) & -\frac{\sqrt{3}}{2}t_{s_2p\sigma}(ik_x - k_y) \\ & & \varepsilon_p + 3(t_{pp\sigma} + t_{pp\pi}) + \lambda & 0 \\ & & & \varepsilon_p + 3(t_{pp\sigma} + t_{pp\pi}) - \lambda \end{pmatrix}, \quad (1)$$

where ε_{s_1}, ε_{s_2} and ε_p are the on-site energies; $t_{s_1s_1\sigma}$, $t_{s_1s_2\sigma}$, $t_{s_2s_2\sigma}$, $t_{s_1p\sigma}$, $t_{s_2p\sigma}$, $t_{pp\sigma}$ and $t_{pp\pi}$ are nearest-neighbor (NN) hopping parameters; λ is SOC strength; k_x and k_y are momenta along x and y directions, respectively. The whole TB Hamiltonian is available in Note 1 in the ESI.†

At the Γ point, the four eigenvalues are $E_{s_1} = \varepsilon_{s_1} + 6t_{s_1s_1\sigma}$, $E_{s_2} = \varepsilon_{s_2} + 6t_{s_2s_2\sigma}$ and $E_p^{\pm\lambda} = E_p \pm \lambda = \varepsilon_p + 3(t_{pp\sigma} + t_{pp\pi}) \pm \lambda$, respectively. E_{s_1} and E_{s_2} are independent of SOC, while E_p is split by SOC with $\Delta E_p^{SOC} = 2\lambda$. As shown in Fig. 1(a), when the extrinsic s_1 band with an appropriate energy is brought into the proximity of intrinsic s_2 p-bands of a 2D semiconductor, an s_1–p band inversion can occur, resulting in a topological phase transition to form the TI phase. Depending on whether the s_1 band inverts with the upper or lower p_x/p_y band, there can be two types of TI phases as indicated by TI(A) and TI(B) in the right panel of Fig. 1(a).

To reveal how the orbital design principle works, we construct phase diagrams [Fig. 1(b)–(d) and Fig. S2–S4†] of the electronic structure with the parameters $\Delta\varepsilon = \varepsilon_{s_1} - \varepsilon_p$ (on-site energy difference between the adsorbate and the anion of the semiconductor), E_g (band gap of the semiconductor without SOC) and λ, based on the above TB model. With an increasing $\Delta\varepsilon$ at given λ and E_g [Fig. 1(b) and (c)], the phase evolves from a metal, TI(B), TI(A), to a normal insulator (NI). The typical band structure of each phase is shown in Fig. S1.† The s_1–p band inversion may or may not exist in the absence of SOC. When SOC is included, the degenerate p_x/p_y valence bands split. As illustrated in Fig. 1(d), this may result in a TI phase with an appropriate $\Delta\varepsilon$, which can be either a TI(A) or TI(B) phase. The condition for the occurrence of the TI (A) or TI(B) phase is determined by the relative magnitude of band splitting $\Delta E_{s_1p} = E_{s_1} - E_p = \Delta\varepsilon - T$ (the s_1/p energy difference at the Γ point without considering SOC as indicated in Fig. 1(a); T is related to hopping parameters) and SOC gap ΔE_p^{SOC}.[3,25] The TI phase can only occur for $\Delta E_{s_1p} < \Delta E_p^{SOC}$, otherwise only NI exists. Furthermore, for $\Delta E_{s_1p} < \Delta E_p^{SOC}$, only TI(A) occurs for $\Delta E_{s_1p} > 0$, where the SOC induces an s_1–p band inversion similar to the case of a small-gap quantum well;[10] for $\Delta E_{s_1p} < 0$, where the s_1–p bands are already inverted and the SOC simply opens a gap similar to graphene,[9] and depending on whether $|\Delta E_{s_1p}|$ is smaller or bigger than ΔE_p^{SOC}, either TI(A) or TI(B) occurs. Apparently, besides $\Delta\varepsilon$, the smaller the E_g [Fig. 1(b) and S3†] or bigger the λ [Fig. 1(c) and S2†] is, the larger the range of the TI phase will be.

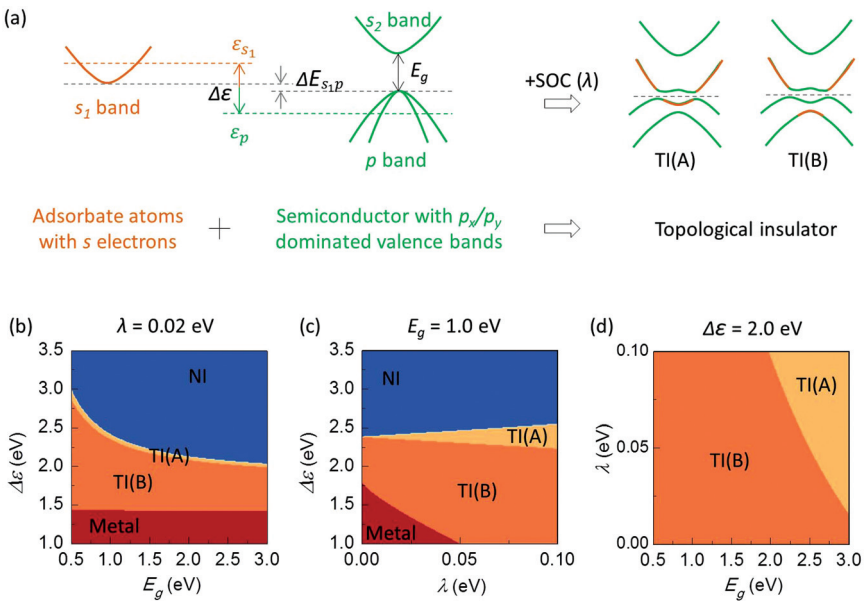

Fig. 1 (a) Schematic illustration of orbital designed TIs from 2D semiconductors. The orange and green solid curves indicate the bands of the adsorbate atom and semiconductor, respectively. The dashed lines in the right panel indicate the Fermi level. TI(A) and TI(B) are defined for the s_1 band inverting with the upper and lower p_x/p_y band, respectively. (b)–(d) Topological phase diagrams in the parameter space of $\Delta\varepsilon$ and E_g, $\Delta\varepsilon$ and λ, λ and E_g, respectively. The other parameters: $t_{s_1s_1\sigma} = t_{s_1s_2\sigma} = t_{s_2s_2\sigma} = -0.25$ eV, $t_{s_1p\sigma} = -0.5$ eV, $t_{s_2p\sigma} = -0.1$ eV, $t_{pp\sigma} = 0.1$ eV, $t_{pp\pi} = 0.01$ eV and $\theta = \pi/3$.

Given the understanding of the orbital design principle based on the TB model, it is natural to ask whether it can be realized in real materials. Recently, experimental fabrication of monolayer CuSe,[26,27] which possesses the p_x/p_y-dominated valence bands, has drawn our attention. The monolayer honeycomb monochalcogenide MX (M = Cu, Ag; X = S, Se, Te) family can all be viewed effectively as "hole-doped" sp-band 2D semiconductors, with one electron depleted per unit cell as shown in Fig. S5.† It is expected that adsorption of one alkali atom per unit cell, which introduces one electron from the s-orbital (s_1-state), will move the Fermi level up to the top of the valence band and result in a semiconductor. Furthermore, if the energy of the s_1-state of alkali atoms is right relative to the top of the valence p-band of the semiconductor, the TI phase can be realized under certain conditions based on the above design principle.

Therefore, the key is to identify the right alkali element with an appropriate s_1-state energy for a given 2D semiconductor, such as CuSe with the known valence p-band position and SOC strength. Because of the level repulsion, the relative position of final s_1 and p bands is also affected by the bottom of the conduction s_2 band. So, based on the above TB model, we construct a phase diagram for the ε_{s_1} of the adsorbate in the parameter space of ε_{s_2} and ε_p of the semiconductor, as shown in Fig. 2(a). It is found that the ε_{s_1} of the adsorbate decreases when the ε_{s_2} (ε_p) of the cation (anion) in the compound semiconductor decreases (increases). Note that a decreased $\varepsilon_{s_1}/\varepsilon_{s_2}$ and ε_p means an increasing ability of donating and accepting electrons, respectively. That is, with the ability of donating (accepting) electrons for the cation (anion) increasing (decreasing) in the semiconductor, the adsorbate to be chosen should have an increasing ability of donating electrons. Taking CuS, CuSe and CuTe as examples, which have the same cation but different anions, the ability of accepting electrons decreases from S, Se to Te, so the adsorbate should have an increasing ability of donating electrons.

To confirm the above hypothesis, first-principles calculations (see Note 2 in the ESI† for details) have been performed for CuS, CuSe and CuTe with different alkali adsorbates. Alkali atoms prefer to be adsorbed at the center of the hexagon as shown in Fig. 2(b). The "p-type" semiconductors CuS and CuTe [Fig. 2(c) and (d)] have been successfully converted into TIs [Fig. 2(e)–(h)] *via* Na and K adsorption, respectively. Without considering SOC, the two degenerate p_x/p_y bands are exactly at the Fermi level. And the s_1 band of the adsorbate is below the p_x/p_y bands of the host semiconductor near the Γ point, leading to "pre-existing" band inversion. When SOC is included, the degenerate p_x/p_y bands split with ΔE_p^{SOC}, resulting in TI(B) and TI(A) phases for CuS-Na and CuTe-K, respectively. The ability of accepting electrons decreases from S to Te while the ability of donating electrons increases from Na to K, in good agreement with the prediction based on the orbital design principle.

Next, we further investigate the band structures of CuSe-Na [Fig. 3(a) and (b)] and CuSe-K [Fig. 3(c) and (d)], which are a NI and metal respectively. Because the ability of donating electrons for Se is between that for S and Te, the ε_{s_1} of Na (K) is too big (small) to convert CuSe into a TI. Thus, according to the phase diagram [Fig. 2(a)], the appropriate ε_{s_1} is between that of Na and K, indicating that adsorbing a mixture of Na and K with a tuned s_1-level energy may convert CuSe into a TI. This is indeed confirmed by calculations of CuSe *via* adsorbing mixtures of Na and K with different ratios as shown in Fig. 3(e)–(g). With the decrease of the Na/K ratio, the s_1 band moves downward at the Γ point and the band structure evolves from CuSe-Na to CuSerK with the band inversion occurring at CuSe-$Na_{0.5}K_{0.5}$. When SOC is included, CuSe-$Na_{0.5}K_{0.5}$ is found to be a TI possessing a non-trivial gap of 41 meV as shown in Fig. 3(h).

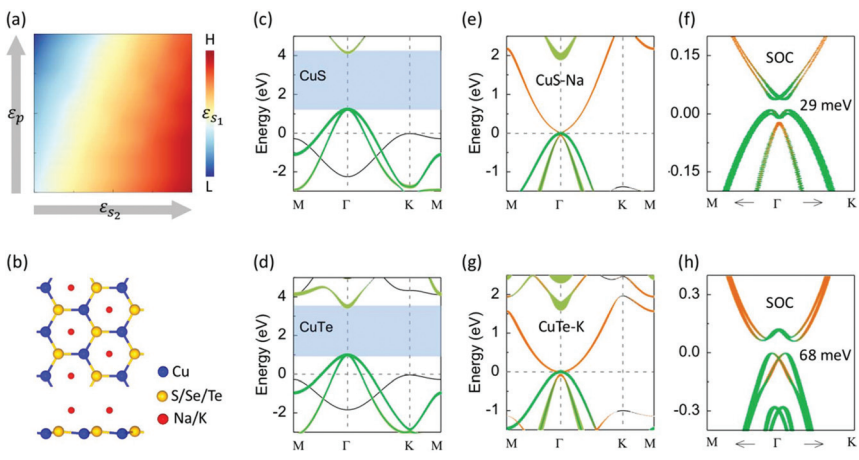

Fig. 2 (a) Phase diagram of appropriate ε_{s_1} in the parameter space of ε_{s_2} and ε_p. The color indicates the value of ε_{s_1}. And an increased on-site energy (ε_{s_1}, ε_{s_2} and ε_p) means a decreasing ability of donating or accepting electrons. (b) Top and side views of monolayer MX–Y (M = Cu; X = S, Se, Te; Y = Na, K). (c)–(f) Projected band structures without SOC of CuS, CuTe, CuS-Na and CuTe-K, respectively. (g) and (h) Projected band structures with SOC of CuS-Na and CuTe-K, respectively. The width of colored lines represents the contribution from different orbitals. The components of the X-s (X = Na, K) states are multiplied by a factor of 4 for clarity. The numbers indicate the band gap.

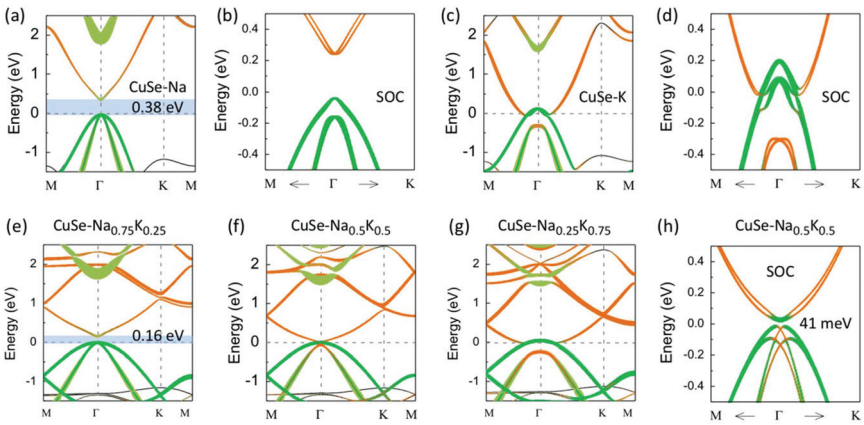

Fig. 3 (a)–(d) Projected band structures without and with SOC of CuSe-Na and CuSe-K, respectively. (e)–(g) Projected band structures without SOC of CuSe-$Na_{0.75}K_{0.25}$, CuSe-$Na_{0.5}K_{0.5}$ and CuSe-$Na_{0.25}K_{0.75}$, respectively. (h) Projected band structures with SOC of CuSe-$Na_{0.5}K_{0.5}$. The width of colored lines represents the contribution from different orbitals. The components of the X-s (X = Na, K) states are multiplied by a factor of 4 for clarity. The numbers indicate the band gap.

Besides tuning the s_1 band *via* adsorbing different alkali elements, one can also slightly tune the p_x/p_y valence bands of the host semiconductor *via* strain so as to achieve a desired ΔE_{s_1p}. For example, CuSe-Na is a NI. By applying a compressive strain, the relative energy of the s_1 band to the p_x/p_y bands decreases near the Γ point (Fig. S6†). Then, the phase evolves from a NI, TI(A), TI(B) to a metal with the increasing strain (Fig. S6†). The specific band structure of TI(A) and TI(B) phases is shown in Fig. 4(a) and (b), respectively, for CuSe-Na with −2.6% and −4% compressive strain. To convert CuSe-Na into a TI, the range of compressive strain is about −2.3% to −4.5%.

Similarly, CuSe-K is a metal. By applying a tensile strain, the relative energy of the s_1 band to the p_x/p_y bands increases near the Γ point (Fig. S7†). The phase evolves from a metal, TI (B), TI(A) to a NI with the increasing strain (Fig. S7†). The specific band structure of TI(B) and TI(A) phases is shown in Fig. 4(c) and (d), respectively, for CuSe-K with 2% and 3.4% tensile strain. To convert CuSe-K into a TI, the range of tensile strain is about 1%–3.6%. To comfirm that the s_1–p inverted bands display topological insulating states, taking CuSe-K with 3% tensile strain as an example, we calculated its nontrivial edge states as shown in Fig. S8.†

We have also tried out using Rb and Cs as adsorbates and found that CuSe-Cs, CuTe-Rb and CuTe-Cs are 2D TIs, as shown in Fig. S9.† Furthermore, taking the alkali atom adsorbed CuX (X = S, Se, Te) monolayers as examples, we further checked their stability. The calculated phonon dispersion of these monolayers is shown in Fig. S10.† There is no imaginary frequency mode in the whole Brillouin zone, indicating that they are dynamically stable.

In conclusion, we propose a novel approach underlined by an orbital design principle, to rationally convert 2D sp-band

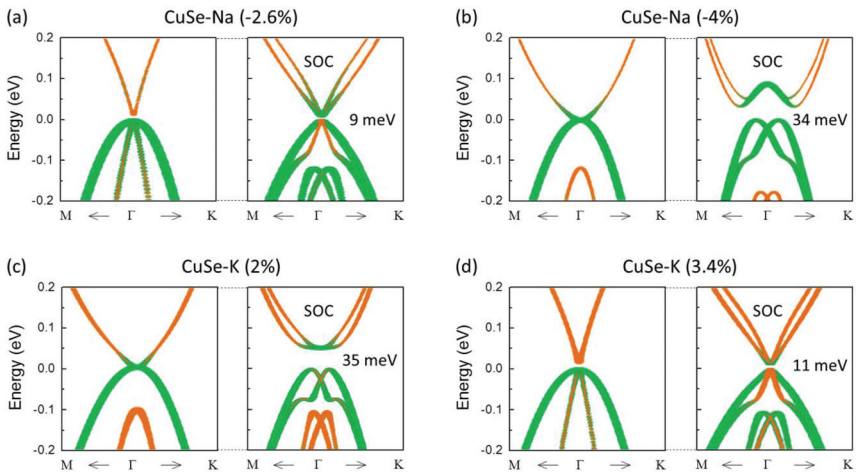

Fig. 4 (a) and (b) Projected band structures of CuSe-Na with −2.6% and −4% compressive strain, respectively. (c) and (d) Projected band structures of CuSe-K with 2% and 3.4% tensile strain, respectively. The width of colored lines represents the contribution from different orbitals. The components of the X-s (X = Na, K) states are multiplied by a factor of 4 for clarity. The numbers indicate the band gap.

semiconductors into TIs. We envision that this approach is generally applicable to a large number of 2D material databases. As prototypical examples, the feasibility of the approach is confirmed by first-principles calculations of monolayer CuX (X = S, Se, Te) *via* adsorbing alkali atoms. Depending on the desired relative position of the extrinsic s-band of alkali atoms to the intrinsic top of the p-valence band of the host, a mixture of alkali atoms and either tensile or compressive strains may be needed. Our findings not only enrich 2D TIs with new material classes but also revive the discovery of TIs by predictive material designs.

Conflicts of interest

There are no conflicts to declare.

Acknowledgements

This work was financially supported by the National Key Research and Development Projects of China (2016YFA0202300), Strategic Priority Research Program of Chinese Academy of Sciences (Grant No. XDB30000000 and XDB07030100), the National Natural Science Foundation of China (No. 51872284 and 61888102), the International Partnership Program of Chinese Academy of Sciences (No. 112111KYSB20160061), and the CAS Pioneer Hundred Talents Program, Beijing Nova Program (No. Z181100006218023). This project was also supported by the CAS Key Laboratory of Vacuum Physics and the Beijing Key Laboratory for Nanomaterials and Nanodevices. G. S. and F. L. at Utah acknowledge the support from US-DOE (Grant No. DE-FG02-04ER46148).

References

1 S. D. Sarma, S. Adam, E. H. Hwang and E. Rossi, *Rev. Mod. Phys.*, 2011, **83**, 407–470.
2 A. K. Geim and I. V. Grigorieva, *Nature*, 2013, **499**, 419–425.
3 Z. F. Wang, K.-H. Jin and F. Liu, *Wiley Interdiscip. Rev.: Comput. Mol. Sci.*, 2017, **7**, e1304.
4 G. Li, Y. Y. Zhang, H. Guo, L. Huang, H. Lu, X. Lin, Y. L. Wang, S. Du and H. J. Gao, *Chem. Soc. Rev.*, 2018, **47**, 6073–6100.
5 K. S. Novoselov, A. K. Geim, S. V. Morozov, D. Jiang, M. I. Katsnelson, I. V. Grigorieva, S. V. Dubonos and A. A. Firsov, *Nature*, 2005, **438**, 197–200.
6 Y. B. Zhang, Y. W. Tan, H. L. Stormer and P. Kim, *Nature*, 2005, **438**, 201–204.
7 F. Xia, H. Wang and Y. Jia, *Nat. Commun.*, 2014, **5**, 4458.
8 K. S. Novoselov, D. Jiang, F. Schedin, T. J. Booth, V. V. Khotkevich, S. V. Morozov and A. K. Geim, *Proc. Natl. Acad. Sci. U. S. A.*, 2005, **102**, 10451–10453.
9 C. L. Kane and E. J. Mele, *Phys. Rev. Lett.*, 2005, **95**, 226801.
10 B. A. Bernevig, T. L. Hughes and S. C. Zhang, *Science*, 2006, **314**, 1757–1761.
11 F. Reis, G. Li, L. Dudy, M. Bauernfeind, S. Glass, W. Hanke, R. Thomale, J. Schäfer and R. Claessen, *Science*, 2017, **357**, 287.
12 L. Kou, Y. Ma, Z. Sun, T. Heine and C. Chen, *J. Phys. Chem. Lett.*, 2017, **8**, 1905–1919.
13 Q.-Y. Wang, Z. Li, W.-H. Zhang, Z.-C. Zhang, J.-S. Zhang, W. Li, H. Ding, Y.-B. Ou, P. Deng, K. Chang, J. Wen, C.-L. Song, K. He, J.-F. Jia, S.-H. Ji, Y.-Y. Wang, L.-L. Wang, X. Chen, X.-C. Ma and Q.-K. Xue, *Chin. Phys. Lett.*, 2012, **29**, 037402.
14 B. Huang, G. Clark, E. Navarro-Moratalla, D. R. Klein, R. Cheng, K. L. Seyler, D. Zhong, E. Schmidgall, M. A. McGuire, D. H. Cobden, W. Yao, D. Xiao, P. Jarillo-Herrero and X. Xu, *Nature*, 2017, **546**, 270–273.
15 Z. F. Wang, Z. Liu and F. Liu, *Phys. Rev. Lett.*, 2013, **110**, 196801.
16 Z. F. Wang, Z. Liu and F. Liu, *Nat. Commun.*, 2013, **4**, 1471.
17 X. Zhang, Y. Zhou, B. Cui, M. Zhao and F. Liu, *Nano Lett.*, 2017, **17**, 6166–6170.
18 E. Jin, M. Asada, Q. Xu, S. Dalapati, M. A. Addicoat, M. A. Brady, H. Xu, T. Nakamura, T. Heine, Q. Chen and D. Jiang, *Science*, 2017, **357**, 673–676.
19 C. Si, Z. Liu, W. Duan and F. Liu, *Phys. Rev. Lett.*, 2013, **111**, 196802.
20 B. Huang, M. Yoon, B. G. Sumpter, S. H. Wei and F. Liu, *Phys. Rev. Lett.*, 2015, **115**, 126806.
21 C. Tan, X. Cao, X. J. Wu, Q. He, J. Yang, X. Zhang, J. Chen, W. Zhao, S. Han, G. H. Nam, M. Sindoro and H. Zhang, *Chem. Rev.*, 2017, **117**, 6225–6331.
22 Z. F. Wang, Y. Zhang and F. Liu, *Phys. Rev. B: Condens. Matter Mater. Phys.*, 2011, **83**, 041403.
23 Y. Zhang and F. Liu, *Appl. Phys. Lett.*, 2011, **99**, 241908.
24 C. Si, Z. Sun and F. Liu, *Nanoscale*, 2016, **8**, 3207–3217.
25 Z. F. Wang, K. H. Jin and F. Liu, *Nat. Commun.*, 2016, **7**, 12746.
26 X. Lin, J. C. Lu, Y. Shao, Y. Y. Zhang, X. Wu, J. B. Pan, L. Gao, S. Y. Zhu, K. Qian, Y. F. Zhang, D. L. Bao, L. F. Li, Y. Q. Wang, Z. L. Liu, J. T. Sun, T. Lei, C. Liu, J. O. Wang, K. Ibrahim, D. N. Leonard, W. Zhou, H. M. Guo, Y. L. Wang, S. X. Du, S. T. Pantelides and H. J. Gao, *Nat. Mater.*, 2017, **16**, 717–721.
27 L. Gao, J. T. Sun, J. C. Lu, H. Li, K. Qian, S. Zhang, Y. Y. Zhang, T. Qian, H. Ding, X. Lin, S. Du and H. J. Gao, *Adv. Mater.*, 2018, **30**, 1707055.